www.jcimcr.org

JCIMCR OPEN ACCESS Journal of Clinical Images and Medical Case Reports

ISSN 2766-7820

Research Article

Open Access, Volume 3

Predicting hemodynamic performance of Fontan Operation for Glenn physiology using computational fluid dynamics: Ten patient-specific cases

Elahe Javadi[1]; Sebastian Laudenschlager[2]; Vitaly Kheyfets[3]; Michael Di Maria[4]; Matthew Stone[5]; Safa Jamali[1]; Andrew J Powell[5]; Mehdi H Moghari[2]

[1]Mechanical and Industrial Engineering Department, Northeastern University, Boston, MA, USA.

[2]School of Medicine, University of Colorado Aurora, and Department of Radiology, Children's Hospital Colorado, Aurora, CO, USA.

[3]Paediatric Critical Care Medicine, Developmental Lung Biology and CVP Research Laboratories, School of Medicine, University of Colorado, Aurora, CO, USA.

[4]Department of Pediatrics, University of Colorado, and Department of Cardiology, Children's Hospital Colorado, Aurora, CO, USA.

[5]Department of Surgery, University of Colorado, and Children's Hospital Colorado, Aurora, CO, USA.

[6]Department of Cardiology, Boston Children's Hospital, Boston, MA, USA.

***Corresponding Author: Elahe Javadi, PhD**
Mechanical and Industrial Engineering Department
Northeastern University, 360 Huntington Ave, Boston, MA 02115, USA.
Email: Javadi.e@northeastern.edu

Received: May 21, 2022
Accepted: Jun 22, 2022
Published: Jun 29, 2022
Archived: www.jcimcr.org

DOI: www.doi.org/10.52768/2766-7820/1916

Keywords: Simulation of cardiac surgeries; Fontan operation; Single-ventricle; Cardiac MRI; Catheterization; Computational fluid dynamics; Blood flow.

Abstract

Single ventricle hearts have only one ventricle that can pump blood effectively and the treatment requires three stages of operations to reconfigure the heart and circulatory system. At the second stage, Glenn procedure is performed to connect Superior Vena Cava (SVC) to the Pulmonary Arteries (PA). For the third and most complex operation, called Fontan, an extracardiac conduit is used to connect Inferior Vena Cava (IVC) to the PL and there after no deoxygenated blood goes to the heart.

Predicting Hemodynamic Performance of Fontan Operation using Computational Fluid Dynamics (CFD) is hypothesized to improve outcomes and optimize this treatment planning in children with single-ventricle heart disease. An important reason for this surgical planning is to reduce the development of Pulmonary Arteriovenous Malformations (PAVM) and the need to perform Fontan revisions. The purpose of this study was to develop a model for Fontan surgical planning and use this model to compare blood circulation in two designed graft types of Fontan operation known as T-shape and Y-graft. The functionality of grafts was compared in terms of Power Loss (PL) and Hepatic Flow Distribution (HFD), a known factor in PAVM development.

To perform this study, ten single-ventricle children with Glenn physiology were included and a CFD model was developed to estimate the blood flow circulation to the left and right pulmonary arteries. The estimated blood flow by CFD was compared with that measured by cardiovascular magnetic resonance. Results showed that there was an excellent agreement between the net blood flow in the right and left pulmonary arteries computed by CFD and CMR (ICC= 0.98, P-value ≥0.21).

After validating the accuracy of each CFD model, Fontan operations using T-shape and Y-graft conduits were performed in silico for each patient and the developed CFD model was used to predict the post-surgical PL and HFD. We found that the PL in the Y-graft was significantly lower than in the T-shape (P-value ≤0.001) and HFD was significantly better balanced in Y-graft compared to the T-shape (P-value=0.004).

Citation: Javadi E, Laudenschlager S, Kheyfets V, Di Maria M, Stone M, et al. Predicting hemodynamic performance of Fontan Operation for Glenn physiology using computational fluid dynamics: Ten patient-specific cases. J Clin Images Med Case Rep. 2022; 3(6): 1916.

Introduction

Staged surgical palliation for patients with single-ventricle heart disease seeks to eventually arrange the systemic and pulmonary circulations in series, using the single-ventricle to pump blood to the systemic circulation [1]. This sequence of surgeries includes the (1) Norwood operation; (2) the bidirectional Glenn operation; and (3) the Fontan completion resulting in a Total Cavopulmonary Connection (TCPC), where the Inferior Vena Cava (IVC) and Superior Vena Cava (SVC) are connected to The Right and Left Pulmonary Arteries (RPA and LPA) and bypass the heart [2].

Although the TCPC provides an improvement over previous Fontan designs, patients are still affected by long-term complications [3,4]. Some of these complications are related to the hemodynamic performance of the TCPC design. Increased Power Losses (PL) across the connection of TCPC have been related to the decreased exercise capability of single-ventricle patients [5]. In addition, unbalanced Hepatic Flow Distribution (HFD) to the left and right lungs may lead to the development of pulmonary arteriovenous malformations [6,7].

Therefore, it is important to optimally design the TCPC connection to have a minimum PL and an even HFD to the left and right lungs. Previous studies have focused on hemodynamic efficiency, not only trying to minimize the PL across the TCPC with T-shape connection type but also improving the HFD [8-11]. For example, the Y-graft Fontan [12,13], a modification of the T-shape based on Soerensen's Opti Flo [14], has been developed and implemented. In Y-graft design, collision of the SVC and IVC blood flow is avoided by placing the two branches of Y-graft connection with an offset with respect to SVC. However, the Y-branch placement is sometimes constrained because of an atomical restriction. Some of these restrictions not ably limit options for the surgical approach since they are inherent to the patient's an atomy. However, the location of IVC anastomosis to the RPA and LPA in extracardiac T-shape conduit and Y-graft can be augmented to minimize the PL and balance the HFD to the left and right lungs. Previous studies used Computational Fluid Dynamics (CFD) to modify the extracardiac T-shape and Y-graft conduits to analyze the hemodynamics outcomes [15,16]. These studies, however, have not modeled T-junction and Y-graft structures on the single-ventricle patients with Glenn physiology and compared their resulting hemodynamic outcomes. They have mainly revised and modified the existing Fontan structures to achieve lower PL and more balanced HFD.

In this study, we designed a CFD model for accurately estimating the blood flow circulation to the RPA and LPA in single-ventricle patients with Glenn physiology. We then simulated a Fontan surgery in these patients using both the extracardiac T-junction and Y-graft conduits. The developed CFD model was then used to compare the resulting PL and HFD between these two connections.

Methods

Patient population and imaging exams:

This retrospective study was approved by Institutional Review Board at Boston Children's Hospital (IRB-P00011748). Ten patients (1 female, median age 3.2 years, age range 1.3-5.3 years) with single-ventricle heart disease and a Glenn shunt who had a Cardiovascular Magnetic Resonance (CMR) exam and catheterization on the same day were retrospectively identified. The CMR exam was performed with the patient under anesthesia in part to evaluate the cardiac anatomy and the Glenn pathway, and to measure blood flow in the RPA, LPA, IVC, and superior vena cavae. A free-breathing prospective Electrocardiogram (ECG) and respiratory-gated Three-Dimensional (3D) steady-state free precession sequence was used to image the whole-heart and central mediastinum at end-diastole [17]. A free-breathing 2D phase-contrast spoiled gradient echo sequence was used to measure the blood flow in great vessels including the RPA, LPA, IVC, and superior vena cavae. Immediately after the CMR exam, these patients went to the catheterization laboratory while still under anesthesia where RPA, LPA, and Left and Right Atrium (LA and RA) pressures were measured. Table 1 displays these patients' diagnosis, gender, age, and their measured blood flow by CMR and pressures by catheterization.

CFD model for the estimation of hemodynamics in single-ventricle patients with Glenn physiology

Figure 1A shows the schematic diagram of the developed patient-specific CFD model for the estimation of blood flow in the RPA and LPA in Glenn pathway. First, the axial images from the 3D steady-state free precession sequence from 10 patients were manually segmented using 3D-Slicer software [18] to delineate the superior vena cavae, Glenn pathway, RPA, and LPA. The segmentation results were then used in Ansys meshing software [19] to generate a 3D patient-specific mesh model for each patient (Figure 1B). A non uniform triangular mesh with size of 0.6 mm was chosen after performing a mesh independency study. Ansys Fluent software [20] was then used to perform the CFD simulation and compute the blood flow in the RPA and LPA. Simulations were performed using a pressure integrated algorithm assuming a Newtonian fluid, viscous flow, and a rigid wall with a no slip boundary condition [21]. Blood behaves as a Newtonian fluid in large arteries [22] with the kinematic viscosity of 0.004 $kg{\cdot}m^{-1}{\cdot}s^{-1}$ and fluid density of 1060 kg/m^3 [11].

The inputs to the CFD model, i.e., inlets, were the transient SVC, or Left SVC (LSVC) and Right SVC (RSVC) blood flow from CMR and the proximal RPA and LPA mean pressures measured from catheterization. The outputs of the CFD model, i.e., outlets, were the transient blood flow in the RPA and LPA. To validate the accuracy of the developed CFD model in the estimation of the blood flow in the RPA and LPA, the estimated net blood flow in the RPA and LPA was compared to that measured by CMR.

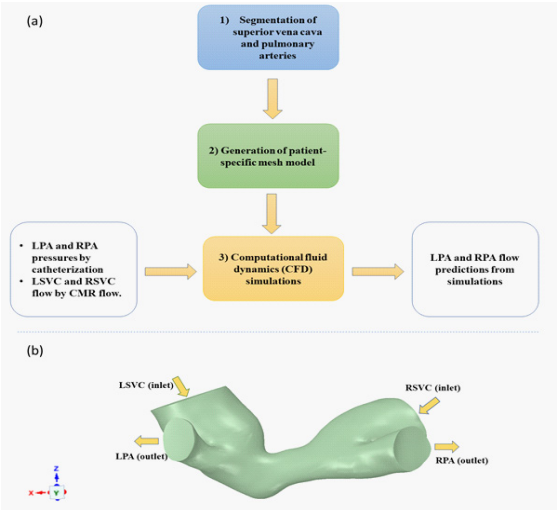

Figure 1: CFD Model for the estimation of hemodynamic parameters in Glenn pathway. (a) CFD simulation workflow and (b) generated 3D model and boundary conditions for one patient. Inputs (i.e., inlets) to the CFD analysis model are Right and Left Superior Vena Cava (RSVC and LSVC) flow by CMR and mean pressure values in the Right and Left Pulmonary Artery (RPA and LPA) by catheterization. Outputs (i.e., outlets) from the CFD analysis model are the time-resolved blood flow in the RPA and LPA. CFD: Computational Fluid Dynamics; CMR: Cardiovascular Magnetic Resonance.

Construction of extracardiac T-shape and Y-graft Fontan Operation on single-ventricle patients with Glenn physiology and estimation of postsurgical PL and HFD

Two types of extracardiac TCPC conduits, T-junction connection and Y-graft, were constructed for each patient. In the T-junction connection, the IVC was connected to branch Pulmonary Artery (PA). The cross section of IVC coming out of the liver was segmented in the 3D-slicer and then a tube with the standard diameter of 12 mm was generated to connect the IVC to the branch PA using Space Claim software (one of the tools of Ansys package). This size of conduit was chosen since the mean IVC diameter for these patients was 12.42 ± 1.5 and the conduit over size diameter shouldn't be more than 20% [23]. Since our goal was to compare the functionality of graft types, a fixed conduit size of 12 mm was chosen for all patients to satisfy the 20% oversize limit. The location of the connection between IVC and branch PA was optimized based on the most possible balanced HFD and applying a surgeon's ideas. For the Y-graft, the standard 12 mm conduit that was connected to IVC was divided into two symmetrical 6 mm conduits and each 6 mm tube was connected to the RPA and LPA. Figure 2 shows an example of constructed T-junction connection and Y-graft in a single-ventricle patient with Glenn physiology.

CFD model for the estimation of hemodynamics in Fontan physiologies

The developed CFD model was used to estimate the PL and HFD to the left and right lungs in the new Fontan physiologies. As shown in Figure 2C, the input to the CFD model was transient IVC and SVC blood flow measured by CMR. Also, LPA and RPA pressures must be set as input, and we needed to estimate them since the real operation has not been performed yet to do the measurement. Pressures can be estimated based on the relationship between the pulmonary artery pressure, total pulmonary artery flow and pulmonary resistance [24].

The right and left pulmonary vascular resistance could be calculated at the Glenn stage. The right pulmonary vascular resistance was calculated as pressure difference between the RPA and pulmonary venous RA divided by the net blood flow at RPA, and the left pulmonary vascular resistance was calculated as the pressure difference between the LPA and pulmonary venous LA divided by the net blood flow at LPA:

$$R_{LPA} = \frac{P_{LPA} - P_{LA}}{Q_{LPA}}, \quad (1)$$

$$R_{RPA} = \frac{P_{RPA} - P_{RA}}{Q_{RPA}}. \quad (2)$$

To calculate the P_LPA and P_RPA, it was assumed that the pulmonary vascular resistance remained unchanged before (i.e., at the Glenn stage) and after the Fontan operation. To perform the CFD simulation on the constructed T-junction and Y-graph Fontan physiology, the pressures of RPA and LPA should be estimated as follows:

$$P_{LPA} = Q_{LPA} \times R_{LPA} + P_{LA} \quad (3)$$

$$P_{RPA} = Q_{RPA} \times R_{RPA} + P_{RA}. \quad (4)$$

$$P_{RPA} = Q_{RPA} \times R_{RPA} + P_{RA}. \quad (4)$$

In these equations, there are four unknowns as P_LPA , P_RPA , Q_LPA ,Q_RPA while P_LAand P_RAwere measured by catheterization. For the very first estimation of P_RPA and P_LPA, if we assume that blood flow split to the right and left lung remain constant, considering the physiology like a parallel circuit (Figure 2), and considering the conservation of mass as

$$Q_{RPA} + Q_{LPA} = Q_{SVC} + Q_{IVC}, \quad (5)$$

Q_RPA and Q_LPA could be found and the first estimation of the pressures as an input to the simulations would be calculated by Equations (3) and (4). These pressures along with the transient blood flow at the SVC (LSVC and RSVC in bilateral cases) and IVC were set as inputs to the CFD model to compute the transient blood flow at the RPA and LPA. The blood flow in the RPA and LPA as outputs of simulation were then used in Equations (3) and (4) to recalculate the pressures. This procedure was repeated until the pressure converged to a specific amount. These pressures were calculated for every Fontan physiology and then were used as an input for the simulations. To analyze the performance of Fontan conduits, PL and HFD were calculated based on the estimated blood flow at the RPA and LPA. The absolute PL was measured as the difference between the hemodynamic energies in the inlets and outlets by [25,26].

$$PL = \sum_{SVC,IVC} Q\left(\bar{P} + \frac{1}{2}\rho.\bar{u}^2\right) - \sum_{RPA,LPA} Q\left(\bar{P} + \frac{1}{2}\rho.\bar{u}^2\right), \quad (5)$$

where $\bar{P}$ denotes the static pressure, ρ is density, Q is flow and $\bar{u}$ is velocity vector.

The HFD was defined as the ratio of IVC blood flow to the RPA and LPA. To calculate HFD, a specified number of seeds (N) were generated at the IVC and then the number of particles at the outlets ("N" _"RPA" " and " "N" _"RPA") were counted and averaged over the last 100 timesteps of CFD simulation [25].

$$HFD_{RPA} = \frac{N_{RPA}}{N}, \quad (6)$$

$$HFD_{LPA} = \frac{N_{RPA}}{N}. \quad (7)$$

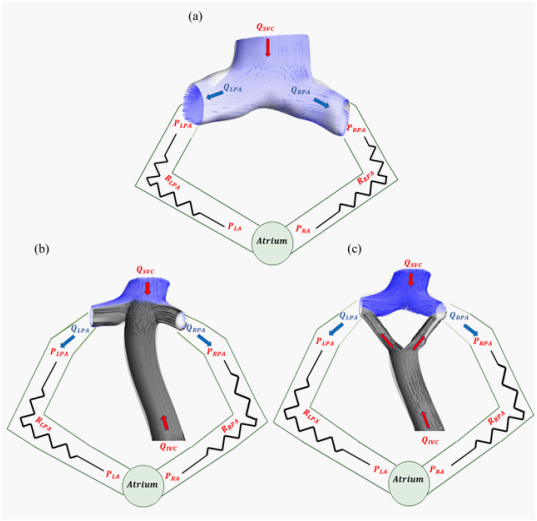

Figure 2: Schematic overview of Glenn physiology (a), Fontan with T-shape conduit (b), and Fontan with Y-graft conduit (c). Q_{LPA}: Flow at Left Pulmonary Artery; Q_{RPA}:Flow At Right Pulmonary Artery; Q_{IVC}: Flow At Inferior Vena Cava; Q_{SVC}: Flow At Superior Vena Cava; P_LPA: Pressure At Left Pulmonary Artery; P_RPA: Pressure At Right Pulmonary Artery; P_{LA}: Pressure at Left Atrium; P_{RA}: Pressure at Right Atrium; R_{LPA}: Pulmonary Vascular Resistance At Left Pulmonary Artery; R_{RPA}: Pulmonary Vascular Resistance at Right Pulmonary Artery.

Statistical Analysis

Descriptive statistics were reported as mean ± standard deviation. The Bland-Altman plot and Intraclass Cross Correlation (ICC) and its 95% Confidence Interval (CI) were calculated for the absolute agreement of a two-way mixed model between the estimated blood flow by CFD and CMR. The normalized mean absolute difference error between the estimated blood flow by CFD and CMR were calculated as $\frac{|CMR_{net\ flow} - CFD_{net\ flow}|}{CMR_{net\ flow}} \times 100$.

The non-parametric Wilcoxon signed-rank test was performed to calculate the P-value. A P-value ≤0.05 was considered statistically significant.

Results

Figure 3 shows the generated patient specific mesh models of 10 patients and the CFD results displaying the blood flow circulation from the SVC (or LSVC and RSVC when both were present) to the RPA and LPA. Figure 4 compares the CFD-simulated transient blood flow in the RPA and LPA with that measured by CMR in all 10 patients. As shown, the CFD model can derive the blood flow measured by CMR at different time points of the cardiac cycle. Although, there was a small discrepancy between the estimated blood flow by CFD and CMR at different cardiac phases, there was no significant difference between the net blood flow in the RPA (0.84 ± 0.31 vs. 0.82 ± 0.27; P-value=0.21) and in the LPA (0.68 ± 0.19 vs. 0.67 ± 0.18; P-value=0.36) measured by CMR and CFD. The maximum difference error between the estimated net blood flow in the RPA and LPA using CFD was less than 10% compared to the CMR (Table 2). Figure 5 demonstrates the Bland-Altman plot between the estimated net blood flow in the RPA and LPA using the CFD and CMR. As shown, there is a slight under estimation of net blood flow by CFD compared to that of CMR (bias ≤2%). There was an excellent agreement between the estimated net blood flow in the RPA using CFD and CMR (ICC=0.98; 95% CI [0.93, 0.99]); and in the LPA using CFD and CMR (ICC=0.98; 95% CI [0.92, 0.99]).

Figures 6 and 7 show the generated T-junction and Y-graft Fontan pathways for the 10 single-ventricle patients with the CFD results showing the blood flow circulation from the IVC and SVC (or LSVC and RSVC when both were present) to the RPA and LPA. The calculated PL and HFD to the left and right lungs in the T-junction and Y-graft Fontan designs are shown in Table 3. On average, the PL was 24% lower and HFD was better balanced between the left and right lungs in the Y-graft compared to the T-junction Fontan construction (Table 3). As shown in Figure 8a, the mean PL for Y-graft was significantly lower than T-junction (5.37 ± 3.77 mW vs. 7.07 ± 4.36 mW; P-value ≤0.001). Figure 8b illustrates that the absolute difference between the HFD to the right and left lungs was significantly lower in the Y-graft compared to the T-junction connection (4.92 ± 2.74% vs. 18.51 ± 12.40%; P-value=0.004).

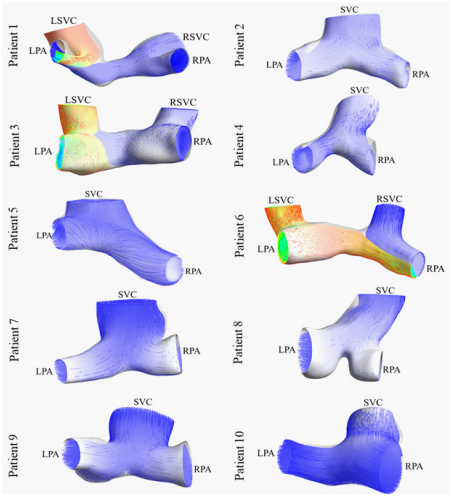

Figure 3: Generated Glenn pathway mesh models for the 10 patients with blood flow streamlines showing the blood flow distributions from the Right and Left Superior Vena Cava (RSVC and LSVC) to the Right and Left Pulmonary Artery (RPA and LPA). The colors indicate estimated blood flow distributions from SVC to RPA and LPA. In patients with bilateral SVCs, red and blue colors display blood flow circulations from LSVC and RSVC, respectively, while in patients with single SVC, only blue color is used. SVC: Superior Vena Cava.

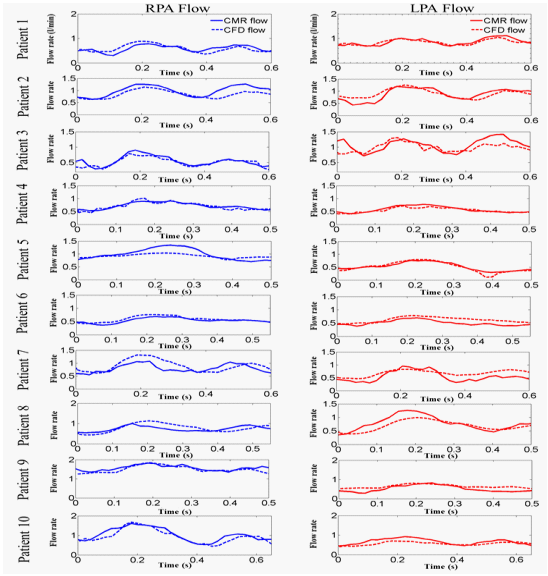

Figure 4: CFD simulated times-series flow curves and CMR-measured time resolved flow curve at RPA and LPA from 10 single-ventricle patients with Glenn physiology. CFD: Computational Fluid Dynamics; CMR: Cardiovascular Magnetic Resonance; LPA and RPA: Left And Right Pulmonary Arteries.

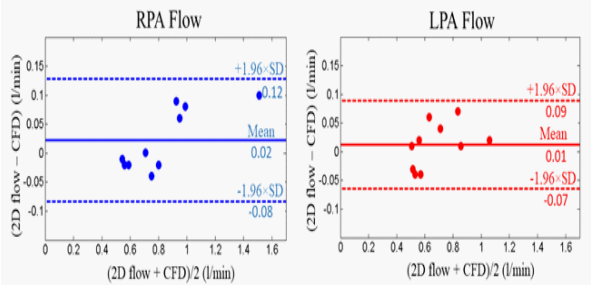

Figure 5: Bland-Altman plot showing the agreement between the CFD-simulated net blood flow and measured CMR net blood flow at the RPA and LPA for all patients. CFD: Computational Fluid Dynamics; CMR: Cardiovascular Magnetic Resonance; LPA: Left Pulmonary Artery; RPA: Right Pulmonary Artery.

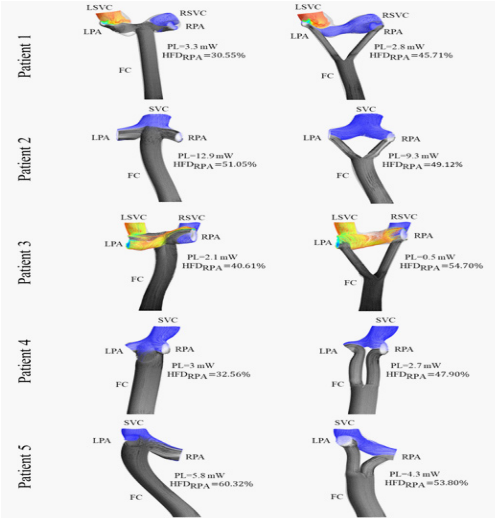

Figure 6: Streamlines of simulated blood flow in constructed T-shape and Y-graft connections for five patients [1-5]. FC: Fontan Conduit; HFD_{RPA}: Hepatic Flow Distribution to the Right Pulmonary Artery; LPA: Left Pulmonary Artery; LSVC: Left Superior Vena Cava; PL: Power Loss; RPA: Right Pulmonary Artery; RSVC: Right Superior Vena Cava; SVC: Superior Vena Cava.

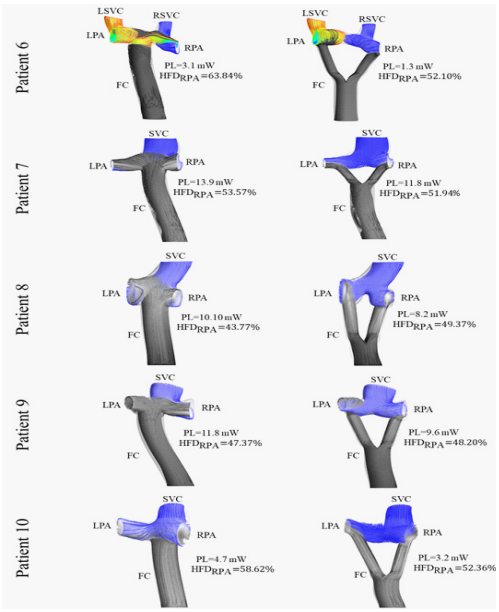

Figure 7: Streamlines of simulated blood flow in constructed T-shape and Y-graft connections for five patients [6-10]. FC: Fontan conduit; HFD_RPA: Hepatic Flow Distribution to the Right Pulmonary Artery; LPA: Left Pulmonary Artery; LSVC: Left Superior Vena Cava; PL: Power Loss; RPA: Right Pulmonary Artery; RSVC: Right Superior Vena Cava; SVC: Superior Vena Cava.

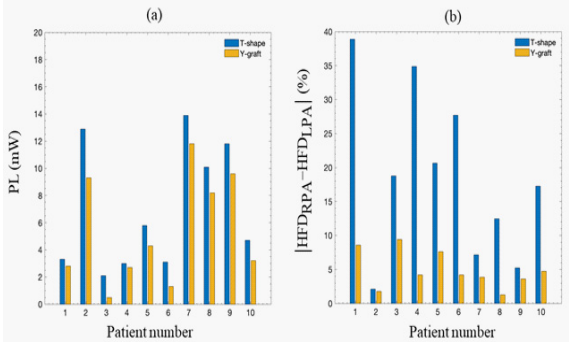

Figure 8: Effect of connection type (T-shape or Y-graft) in Fontan operation on Power Loss (PL) and Hepatic Flow Distribution (HFD) to the left and right pulmonary arteries. Lower PL was observed in Y-graft connection type (a). The HFD to the right (HFD_RPA) and Left Pulmonary Artery (HFD_LPA) is more balanced in Y-graft compared to T-shape (b).

Discussion

This study offers, to the best of our knowledge, the first comparison of prospective T-junction and Y-graft for Fontan surgical planning on single-ventricle children with Glenn physiology. Prior studies have been limited to evaluating patients who had already undergone a Fontan and in whom a Fontan revision was being considered. Our study incorporates data sets from CMR and catheterization to develop a CFD model that accurately estimates the net blood flow distribution to the RPA and LPA with the estimation error of <10% in patients with Glenn physiology. There was slightly higher disagreement between the estimated blood flow by CMR and CFD at different time points of the cardiac cycle, in part likely due to the assumption of rigid wall in our CFD model. Fontan operations were then simulated with patient-specific designed extracardiac T-junction and Y-graft conduits. The developed CFD model was used to predict the postsurgical blood flow distribution to the RPA and LPA and calculate the PL and HFD. Various simulations were performed with different graft placements in the T-junction connection and Y-graft to optimize PL and HFD. It was shown that the PL was lower in Y-graft compared to T-junction connection and the HFD was more evenly balanced in Y-graft. It was also observed that relatively small offsets in graft placement and angulation could largely alter the collisions and interactions among flows from SVC and IVC which affects PL and HFD.

Our method allowed for experimenting with different graft placements and angulations and finding the optimum placement in terms of PL and HFD. The optimal Fontan conduit connection including graft placement and angulation should be precisely replicated by surgeons to achieve the predicted PL and HFD. Any difference between the simulated Fontan conduit connection and the implemented one by surgeons can lead to an error in the predicted PL and HFD. Therefore, if the suggested Fontan conduit can be precisely implemented by surgeons, the developed technique may provide a methodological assessment for the improvement of surgical planning. Although a threshold for HFD to prevent pulmonary arteriovenous malformations is not currently defined, our technique can be used to achieve a balanced HFD through an appropriate Fontan graft conduit connection.

Table 1: Demographic information of each patient in our study along with their CMR and Catheterization data (n=10).

Single-ventricle Patient	Primary Diagnosis	Gender	Age at CMR (Years)	Blood Flow (l/min) Measured by CMR				Pressure (mmHg) Measured by Catheterization			
				RSVC	LSVC	RPA	LPA	RPA	LPA	RA	LA
1	AVCD, BDG, BSVC, DORV	Male	5.30	0.86	0.58	0.86	0.83	13.00	12.00	6.00	5.00
2	BDG, PA, TGA,VSD	Female	5.10	1.84		0.97	0.87	10.00	10.00	6.00	7.00
3	BDG, BSVC, DORV, TGA,VSD	Male	3.90	0.72	0.9	1.07	1.05	12.00	12.00	6.00	6.00
4	AVCD, DORV, PS	Male	1.30	1.28		0.71	0.57	11.00	13.00	7.00	7.00
5	BDG, PA, TGA, VSD	Male	2.10	1.49		0.98	0.51	12.00	12.00	9.00	9.00
6	AVCD, BDG, BSVC, DORV	Male	1.70	0.50	0.54	0.50	0.55	14.00	14.00	8.00	8.00
7	BDG, DILV	Male	2.90	1.34		0.79	0.55	12.00	12.00	8.00	8.00
8	BDG, PA, TGA, VSD	Male	3.40	1.46		0.73	0.73	12.00	13.00	7.00	5.00
9	BDG, VSD	Male	3.60	2.07		1.56	0.51	11.00	11.00	5.00	5.00
10	AVCD, BDG, DORV, PA	Male	3.10	1.69		1.03	0.66	11.00	11.00	6.00	7.00
Mean ± SD			3.24 ± 1.32	1.53 ± 0.29		0.84 ± 0.31	0.68 ± 0.19	11.80 ± 1.13	12.00 ± 1.15	6.80 ± 1.23	6.70 ± 1.42

Data are presented as mean ± standard deviation. AVCD: Atrioventricular Canal Defect; BDG: Bidirectional Glenn; BSVC: Bilateral Superior Vena Cava; CMR: Cardiovascular Magnetic Resonance; DILV: Double Inlet Left Ventricle; DORV: Double Outlet Right Ventricle; LPA: Left Pulmonary Artery; LSVC: Left Superior Vena Cava; PA: Pulmonary Atresia; PS: Pulmonary Stenosis; RPA: Right Pulmonary Artery; RSVC: Right Superior Vena Cava; SV: Stroke Volume; TGA: Transposition of the Great Arteries; VSD: Ventricular Septal Defect.

Table 2: Comparing CFD-simulated flow and CMR-measured flow at RPA and LPA from 10 single-ventricle patients with Glenn physiology.

Patients	Inlet (SVC or RSVC+LSVC)	Outlet (RPA)			Outlet (LPA)		
	2D flow (l/min)	CMR (l/min)	CFD (l/min)	Error (%)	CMR (l/min)	CFD (l/min)	Error (%)
1	1.44	0.58	0.60	3.45	0.86	0.85	1.16
2	1.84	0.97	0.88	9.28	0.87	0.80	8.04
3	1.62	0.55	0.57	3.64	1.07	1.05	1.87
4	1.28	0.71	0.70	1.41	0.57	0.55	3.51
5	1.49	0.98	0.92	6.12	0.51	0.50	1.96
6	1.04	0.54	0.55	1.85	0.50	0.53	6.00
7	1.34	0.79	0.81	2.53	0.55	0.59	7.27
8	1.46	0.73	0.77	5.48	0.73	0.69	5.48
9	2.07	1.56	1.46	6.41	0.51	0.55	7.84
10	1.69	1.03	0.95	7.77	0.66	0.60	9.09
Mean ± SD	1.53 ± 0.29	0.84 ± 0.31	0.82 ± 0.27	4.79 ± 2.63	0.68 ± 0.19	0.67 ± 0.18	5.22 ± 2.90

Data are presented as mean ± Standard deviation. CFD: Computational Fluid Dynamics; CMR: Cardiovascular Magnetic Resonance; LPA: Left Pulmonary Artery; LSVC: Left Superior Vena Cava; RPA: Right Pulmonary Artery; RSVC: Right Superior Vena Cava; SVC: Superior Vena Cava.

$$\text{Error (\%)} = \frac{|CMR_{flow} - CFD_{flow}|}{CMR_{flow}} \times 100.$$

Similar to our study, there have been other attempts to predict and assess PL, HFD, maximum kinetic power, and wall shear stress in Fontan conduit connections. Yang et al. examined the influence of graft size and anastomosis locations on wall shear stress and HFD and illustrated that the performance of the Y-graft design is highly patient-specific and the anastomosis location is likely the most important factor influencing the HFD [30]. Lock et al. showed that customized Fontan designs generated by computer-aided design and optimized by CFD simulations can lead to novel patient specific Fontan conduits and better indexed PL, HFD, and wall shear stress [25]. Trusty et al. investigated the efficacy of a Y-graft Fontan conduit in terms of HFD over time. It was shown that Y-grafts resulted in significantly more balanced HFD over a three year follow up without an increase in TCPC resistance [27]. Although Fontan surgical planning can offer accurate HFD prediction, the same authors showed that improving postoperative anatomy prediction are important to increase the overall accuracy of Fontan surgical planning [28]. Restrepo et al. studied the effect of SVC placement on Y-graft hemodynamics in terms of PL and HFD. It was shown that positioning of SVC plays an important role in the hemodynamic performance of Fontan anatomies and suggested connecting Y-graft branches away from the SVC to minimize the interaction of SVC and IVC flows, and have better flow distribution to the RPA and LPA [29]. Rajabzadeh et al. performed a CFD analysis on T-shaped and Y-grafts and showed a better performance of Y-graft over T-shape [26].

Our approach, however, has some limitations. The patient population is small, and results may vary in a larger patient population. A multicenter study is necessary to increase the number of patients, datasets, and statistical power. In our CFD model, we assumed that the superior vena cava and IVC blood flow as well as pulmonary vascular resistance remained unchanged going from the Glenn stage to Fontan. In addition, our CFD model is mainly based on the data gathered in a resting state and further analysis is necessary to evaluate our model in exercise conditions that may alter PL and HFD [11,12,30-35]. We did not have data after the Fontan operation to validate the estimation of PL and HFD. Our next aim is to follow the results after the Fontan operation and evaluate the accuracy of our model in the prediction of PL and HFD prior to operation. Current methods include only passive static pulmonary circulation, but future efforts can potentially benefit from inclusion of collaterals, elastic vessel walls, systemic circulations, and heart with a fluid structure interaction analysis [35-37]. When a surgeon has selected the surgical option to implement, closely replicating that option in-vivo might be challenging. Some efforts have investigated 3D printing and virtual reality for guiding surgeons, but further improvements are necessary [38]. In addition, patient growth might be important to incorporate into the model to improve surgical planning results.

Conclusions

We developed a CFD model that estimates the blood flow in the LPA and RPA with an estimation error of ≤10% in single-ventricle patients with Glenn physiology. Fontan operations were then simulated with extracardiac T-junction and Y-graft conduits and the CFD model was used to predict the postsurgical PL and HFD. Overall, PL was significantly lower and HFD was significantly more balanced using a Y-graft compared to the T-junction connection. Future efforts and refinements to the surgical planning process will greatly benefit from the inclusion of collaterals, fenestrations, and systemic circulation in both rest and exercise conditions in the model.

Declarations

Funding sources: This work is supported by NIH-NHLBI (1R01HL149807-01 and 5K25 HL 133481).

Conflict of interests: Authors of this study do not have any conflict of interest to declare.

References

1. Fontan F, Baudet E. Surgical repair of tricuspid atresia. Thorax. 1971; 26: 240-248.

2. de Leval, MR, et al. Total cavopulmonary connection: A logical alternative to atriopulmonary connection for complex Fontan operations. Experimental studies and early clinical experience. J Thorac Cardiovasc Surg. 1988; 96: 682-695.

3. Gentles TL, et al. Fontan operation in five hundred consecutive patients: Factors influencing early and late outcome. J Thorac Cardiovasc Surg. 1997; 114:376-391.

4. Chowdhury, UK. et al. Specific issues after extracardiac fontan operation: Ventricular function, growth potential, arrhythmia, and thromboembolism. Ann Thorac Surg. 2005; 80: 665-672.

5. Khiabani, RH, et al. Exercise capacity in single-ventricle patients after Fontan correlates with haemodynamic energy loss in TCPC. Heart. 2015; 101: 139-143.

6. Duncan, B.W. and S. Desai, Pulmonary arteriovenous malformations after cavopulmonary anastomosis. Ann Thorac Surg. 2003; 76: 1759-1766.

7. Shah MJ, et al. Pulmonary AV malformations after superior cavopulmonary connection: resolution after inclusion of hepatic veins in the pulmonary circulation. Ann Thorac Surg. 1997; 63: 960-963.

8. Whitehead KK, et al. Nonlinear power loss during exercise in single-ventricle patients after the Fontan: insights from computational fluid dynamics. Circulation. 2007; 116: I165-1171.

9. Marsden AL, et al. Effects of exercise and respiration on hemodynamic efficiency in CFD simulations of the total cavopulmonary connection. Ann Biomed Eng, 2007; 35: 250-263.

10. Desai K, et al. Haemodynamic comparison of a novel flow-divider Optiflo geometry and a traditional total cavopulmonary connection. Interact Cardiovasc Thorac Surg. 2013; 17: 1-7.

11. Marsden AL, et al. Evaluation of a novel Y-shaped extracardiac Fontan baffle using computational fluid dynamics. The Journal of Thoracic and Cardiovascular Surgery. 2009; 137: 394-403.

12. Haggerty CM, et al. Simulating hemodynamics of the Fontan Y-graft based on patient-specific in vivo connections. The Journal of thoracic and cardiovascular surgery. 2013; 145: 663-670.

13. Kanter KR, et al. Preliminary clinical experience with a bifurcated Y-graft Fontan procedure-A feasibility study. J Thorac Cardiovasc Surg. 2012; 144: 383-389.

14. Soerensen DD, et al. Introduction of a new optimized total cavopulmonary connection. Ann Thorac Surg. 2007; 83: 2182-2190.

15. Baretta A, et al. Virtual surgeries in patients with congenital heart disease: a multi-scale modelling test case. Philos Trans A Math Phys Eng Sci. 2011; 369: 4316-4330.

16. de Zelicourt DA, et al. Individualized computer-based surgical planning to address pulmonary arteriovenous malformations in patients with a single ventricle with an interrupted inferior vena cava and azygous continuation. J Thorac Cardiovasc Surg. 2011;

141: 1170-1177.

17. Moghari MH, Geva T, Powell AJ. Prospective heart tracking for whole-heart magnetic resonance angiography. Magn Reson Med, 2017; 77: 759-765.

18. Pieper S, Halle M, Kikinis R. 3D Slicer. in 2004 2nd IEEE international symposium on biomedical imaging: Nano to macro (IEEE Cat No. 04EX821). 2004. IEEE.

19. Workbench A. Ansys Inc. Canonsburg, PA. Ver. 2009; 12.

20. Fluent A. Ansys fluent. Academic Research. Release. 2015; 14.

21. Issa RI. Solution of the implicitly discretised fluid flow equations by operator-splitting. Journal of computational physics. 1986; 62: 40-65.

22. Pedley TJ, Luo X. Fluid mechanics of large blood vessels. Shaanxi People's Press. 1995.

23. Lemura J. et al. Total extracardiac right heart bypass using a polytetrafluoroethylene graft. Journal of cardiac surgery. 1997; 12: 32-36.

24. Frieberg P, et al. Simulation of aortopulmonary collateral flow in Fontan patients for use in prediction of interventional outcomes. Clinical physiology and functional imaging. 2018; 38: 622-629.

25. Loke YH, et al. Role of surgeon intuition and computer-aided design in Fontan optimization: A computational fluid dynamics simulation study. The Journal of Thoracic and Cardiovascular Surgery, 2020.

26. Rajabzadeh Oghaz H, et al. Pulsatile blood flow in total cavopulmonary connection: A comparison between Y-shaped and T-shaped geometry. Medical & biological engineering & computing. 2017; 55: m213-224.

27. Trusty PM, et al. The first cohort of prospective Fontan surgical planning patients with follow-up data: How accurate is surgical planning? The Journal of thoracic and cardiovascular surgery. 2019. 157: 1146-1155.

28. Trusty PM. et al. Y-graft modification to the Fontan procedure: Increasingly balanced flow over time. The Journal of Thoracic and Cardiovascular Surgery. 2020; 159: 652-661.

29. Restrepo M, et al. Hemodynamic impact of superior vena cava placement in the Y-graft Fontan connection. The Annals of thoracic surgery. 2016; 101: 183-189.

30. Yang W. et al. Hepatic blood flow distribution and performance in conventional and novel Y-graft Fontan geometries: A case series computational fluid dynamics study. The Journal of thoracic and cardiovascular surgery. 2012; 143: 1086-1097.

31. Tang E, et al. Effect of Fontan geometry on exercise haemodynamics and its potential implications. Heart. 2017; 103: 1806-1812.

32. Whitehead KK, et al. Nonlinear power loss during exercise in single-ventricle patients after the Fontan: Insights from computational fluid dynamics. Circulation. 2007; 116: I-165-I-171.

33. Soerensen DD, et al. Introduction of a new optimized total cavopulmonary connection. The Annals of thoracic surgery. 2007; 83: 2182-2190.

34. Khiabani RH, et al. Exercise capacity in single-ventricle patients after Fontan correlates with haemodynamic energy loss in TCPC. Heart. 2015; 101: 139-143.

35. Bossers SS, et al. Computational fluid dynamics in Fontan patients to evaluate power loss during simulated exercise. Heart. 2014; 100: 696-701.

36. Tang E, et al. Fluid-structure interaction simulation of an intra-atrial Fontan connection. Biology. 2020; 9: 412.

37. Rubtsova EN, C Alina, T Dmitry. A mathematical model of the univentricular Fontan. in 2019 IEEE Conference of Russian Young Researchers in Electrical and Electronic Engineering (EIConRus). IEEE. 2019.

38. Carberry T, et al. Fontan revision: Presurgical planning using four-dimensional (4D) flow and three-dimensional (3D) printing. World Journal for Pediatric and Congenital Heart Surgery. 2019; 10: 245-249.